Pancharatnam–Berry phase shaping for control of the transverse enhancement of focusing

Man, Zhongsheng; Dou, Xiujie; Fu, Shenggui

DOI
10.1364/OL.44.000427

Publication date
2019

Document Version
Final published version

Published in
Optics Letters

Optics Letters

Pancharatnam–Berry phase shaping for control of the transverse enhancement of focusing

Zhongsheng Man,[1,2,4] Xiujie Dou,[2,3] and Shenggui Fu[1,5]

[1]School of Physics and Optoelectronic Engineering, Shandong University of Technology, Zibo 255000, China
[2]Optics Research Group, Delft University of Technology, Department of Imaging Physics, Lorentzweg 1, 2628CJ Delft, The Netherlands
[3]Nanophotonics Research Center, Shenzhen University, Shenzhen 518060, China
[4]e-mail: zsman@sdut.edu.cn
[5]e-mail: fushenggui@sdut.edu.cn

Received 14 November 2018; revised 18 December 2018; accepted 19 December 2018; posted 19 December 2018 (Doc. ID 351954); published 14 January 2019

We show that elongating a tightly focused field in the direction perpendicular to the optical axis is possible. We demonstrate our approach by specially shaping the Pancharatnam–Berry (PB) phase. Moreover, the analytical formulae required to calculate the strength vectors and energy flux of the three-dimensional electromagnetic fields near the focus of an aplanatic optical system are derived using the Richards and Wolf vectorial diffraction methods. Calculations reveal that the transverse enhancement is controllable and depend on the phase index in the PB phase, thereby giving rise to a focus with tunable length and subwavelength width in the focal plane.

https://doi.org/10.1364/OL.44.000427

The Pancharatnam–Berry (PB) phase is a well-known geometric phase associated with the polarization of light, first introduced by Pancharatnam in his study of the interference of polarized beams [1]. Berry then pointed out that such a phase appears when the polarization of light traverses a closed loop on the Poincaré sphere [2], where the initial and final states differ by a phase factor equal to half the solid angle encompassed by the loop on the sphere along which the light takes [2–4]. This phase was soon realized to be quite general because it occurs in various systems [5–7]. Most importantly, the PB phase enables the manipulation of light polarization, leading to the creation of vector optical fields with spatially inhomogeneous states of polarization (SoPs) [8,9]. The geometric configuration of SoPs provides an additional and powerful intrinsic degree of freedom (DoF) to control light.

Moreover, there has been currently substantial interest in structured optical fields, that is, the creation of customized optical patterns to satisfy specific needs in all kinds of applications [10–16]. To mention a few examples, a needle of either a longitudinally or transversely polarized beam has been proposed assisted by amplitude, polarization, and phase modulations of the input light in tight focusing systems [10,15], wherein the electric field permits a significant enhancement along the optical axis but suppression in the transverse direction, resulting in a tighter hot spot with long depth of focus. Complex optical longitudinal polarization structures were demonstrated [11]. The reverse flux of light energy was obtained [16]. Last but not least, a Möbius strip in the polarization of light was also achieved [12]. To date, however, attempts to target transverse elongation of the focus in the focal plane have not been undertaken. This is highly desired in practical applications, due to the great potential for promoting imaging speed with a layer-divided imaging scheme and manipulating particles with different length, as well as optical microfabrication and nanofabrication.

In this Letter, we propose a method to elongate the tightly focused field in the direction perpendicular to the optical axis assisted by PB-phase shaping. The expressions for calculating the electromagnetic strength vectors and energy flux near focus are derived using the vectorial diffraction methods of Richards and Wolf. Based on an analytical model, the transverse enhancement was found to depend only on the phase index of the PB phase. As a result, a focus with controllable length and subwavelength width in the focal plane is achieved. Furthermore, the corresponding Poynting vector distributions are studied in detail to provide a better understanding of the transverse enhancement of focusing.

To give a clear understanding of the PB phases, a brief analysis concerning its origin is necessary. Because PB phases are related to variations in the SoPs, we assume there are two polarization states in terms of an initial one $\mathbf{E}_1$ and a final one $\mathbf{E}_2$. For simplicity and without loss of generality, $\mathbf{E}_1$ corresponds to a linear polarization with an orientation with respect to the x axis denoted by c. Hence, it may be represented as a two-dimensional Jones vector such that

$$\mathbf{E}_1 = \cos c\hat{\mathbf{e}}_x + \sin c\hat{\mathbf{e}}_y = \frac{1}{\sqrt{2}}[\exp(-ic)\hat{\mathbf{e}}_l + \exp(ic)\hat{\mathbf{e}}_r], \quad (1)$$

where $\hat{\mathbf{e}}_x$ and $\hat{\mathbf{e}}_y$ denote unit vectors directed along the x and y axes, respectively, of the linear polarization; similarly, $\hat{\mathbf{e}}_l$ and $\hat{\mathbf{e}}_r$ denote unit vectors of left-handed (LH) and right-handed (RH) circular polarization. For arbitrary light beams with a homogeneously linear SoP, the two components expressed in terms

of LH and RH circular vibrations have opposite initial phases, the value of which determines the orientation of the linear vibration. After a polarization transformation, if the PB phases acquired by the LH and RH circular components are, respectively, ε_l and ε_r, the resultant final polarization state $\mathbf{E}_2$ is then expressed as [17]

$$\begin{aligned}\mathbf{E}_2 &= \frac{1}{\sqrt{2}}\{\exp[i(\varepsilon_l - c)]\hat{\mathbf{e}}_l + \exp[i(\varepsilon_r + c)]\hat{\mathbf{e}}_r\} \\ &= e^{\left(i\frac{\varepsilon_r+\varepsilon_l}{2}\right)}\left\{\left[\cos\left(\frac{\varepsilon_r-\varepsilon_l}{2}+c\right)\right]\hat{\mathbf{e}}_x + \left[\sin\left(\frac{\varepsilon_r-\varepsilon_l}{2}+c\right)\right]\hat{\mathbf{e}}_y\right\}.\end{aligned} \tag{2}$$

Unfortunately, a dynamic phase appears in Eq. (2), indicating a phase retardation of $(\varepsilon_r + \varepsilon_l)/2$ compared to that in Eq. (1). However, if we choose $\varepsilon_r = -\varepsilon_l = \varepsilon_e$, this phase disappears. The PB phase ε as an intrinsic optical DoF may have arbitrary distributions in theory, and thus provides a powerful means to manipulate light. Indeed, great success has been achieved in enabling transformations from states $\mathbf{E}_1$ to $\mathbf{E}_2$, such as wave plates and subwavelength gratings as well as specially designed optical systems [8,9,18,19].

Numerous practical applications ranging from microscopy to data storage as well as micromanipulation require tight focusing. Different from previous results suggesting tightly focused fields permit a significant enhancement in the direction along the optical axis, a tunable enhancement in the direction perpendicular to the latter is found also to be possible when setting $\varepsilon_e = 2\pi v(r \sin\varphi/r_0)^3$, where v is the phase index, r and φ denote the polar radius and azimuthal angle, respectively, and r_0 is the radius of the input field. In this case, ε_e is a function of both r and φ; thus, the resultant PB phase gets a space-variant distribution. The corresponding three-dimensional electric field near the focus is derived using Richards–Wolf vectorial diffraction integration [20],

$$\begin{aligned}\mathbf{E}_{\text{out}}(\rho,\phi,z) = \frac{-ikf}{2\pi}\int_0^{2\pi}\int_0^{\alpha}\sqrt{\cos\theta}\,l_{\text{in}}(\theta)\sin\theta\mathbf{M}_e \\ \times e^{\{ik[-\rho\sin\theta\cos(\varphi-\phi)+z\cos\theta]\}}\mathrm{d}\varphi\mathrm{d}\theta,\end{aligned} \tag{3}$$

where (ρ,φ,z) are the cylindrical coordinates of the image space; k and f denote the wave number and focal length, respectively; θ is the tangential angle with respect to the z axis; and $\alpha = \arcsin(\mathrm{NA}/n)$, with NA the numerical aperture of the focusing objective lens and n the refractive index in the image space, which we take as 0.95 and 1, respectively. The function $l_{\text{in}}(\theta)$ represents the complex amplitude distribution of the incident beam, having the form [21]

$$l_{\text{in}}(\theta) = \exp\left[-\beta^2\left(\frac{\sin\theta}{\sin\alpha}\right)^2\right]J_1\left(2\beta\frac{\sin\theta}{\sin\alpha}\right). \tag{4}$$

Here, β is the ratio of the pupil radius to the beam waist, which we choose as 1 in our configuration; $J_1(x)$ is the first kind of first-order Bessel function.

In Eq. (3), $\mathbf{M}_e$ represents the electric field polarization vector in the image space contributed by the input polarization; its explicit form is

$$\mathbf{M}_e = M_{ex}\hat{\mathbf{e}}_x + M_{ey}\hat{\mathbf{e}}_y + M_{ez}\hat{\mathbf{e}}_z, \tag{5}$$

$$\begin{aligned}M_{ex} = \sin\left[\varphi - 2\pi v\left(\frac{\sin\theta\sin\varphi}{\sin\alpha}\right)^3 - c\right]\sin\varphi \\ + \cos\left[2\pi v\left(\frac{\sin\theta\sin\varphi}{\sin\alpha}\right)^3 + c - \varphi\right]\cos\theta\cos\varphi,\end{aligned} \tag{6}$$

$$\begin{aligned}M_{ey} = -\sin\left[\varphi - 2\pi v\left(\frac{\sin\theta\sin\varphi}{\sin\alpha}\right)^3 - c\right]\cos\varphi \\ + \cos\left[2\pi v\left(\frac{\sin\theta\sin\varphi}{\sin\alpha}\right)^3 + c - \varphi\right]\cos\theta\sin\varphi,\end{aligned} \tag{7}$$

$$M_{ez} = \cos\left[2\pi v\left(\frac{\sin\theta\sin\varphi}{\sin\alpha}\right)^3 + c - \varphi\right]\sin\theta. \tag{8}$$

Next, we analyze the tightly focused electric field distributions based on Eqs. (3)–(8). As examples, we explore the focal behaviors of three different optical fields with $(v,c) = (0,\pi/2)$, $(1,\pi/2)$, and $(20,\pi/2)$; the corresponding input polarization and intensity distributions are depicted in Fig. 1, with the focusing conditions mentioned above. For $(v,c) = (0,\pi/2)$ [Fig. 1(a)], the beam is linearly polarized with spatially invariant SoPs. Its orientation is parallel to the y axis direction. However, for a nonzero value of v, the beam has a spatially varying SoP [Figs. 1(b) and 1(c)], with the orientation of the local vibration varying along the y axis but has no change in the direction perpendicular to it. The corresponding normalized electric field distributions in the focal plane are depicted in Fig. 2. Apparently, the y-polarized component [Figs. 2(b), 2(f), and 2(g)] compared to the x-polarized [Figs. 2(a), 2(e), and 2(i)] and z-polarized components [Figs. 2(c), 2(g), and 2(k)] is much stronger and dominates the total field for all the three cases. Specifically, almost no field is found for the x-polarized component [Fig. 2(a)] of the linearly polarized input beam. However, the on-axis quasi-circular intensity distribution for the y-polarized component [Fig. 2(b)] and twin focal spots located along the y axis for the z-polarized component [Fig. 2(c)] play a dominant role, resulting in an elliptically shaped pattern for the total field [Fig. 2(d)] with the major-axis direction being in accordance with the orientation of the input field [Fig. 1(a)]. Most importantly, all three polarization components [Figs. 2(e)–2(g) and 2(i)–2(k)] permit a significant transverse enhancement along the y axis with increasing v, resulting in a tunable length of focus (DoF) in the direction perpendicular to the optical axis for the total field [Figs. 2(h) and 2(l)] accompanied with the increase of side lobes.

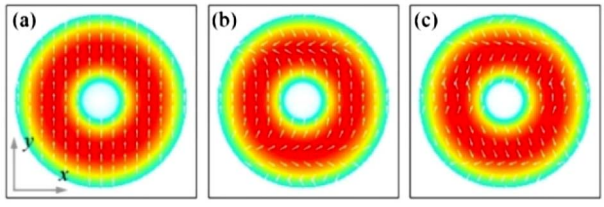

Fig. 1. Polarization and intensity distributions of three different input optical fields with (v, c) = (a) $(0, \pi/2)$, (b) $(1, \pi/2)$, and (c) $(20, \pi/2)$.

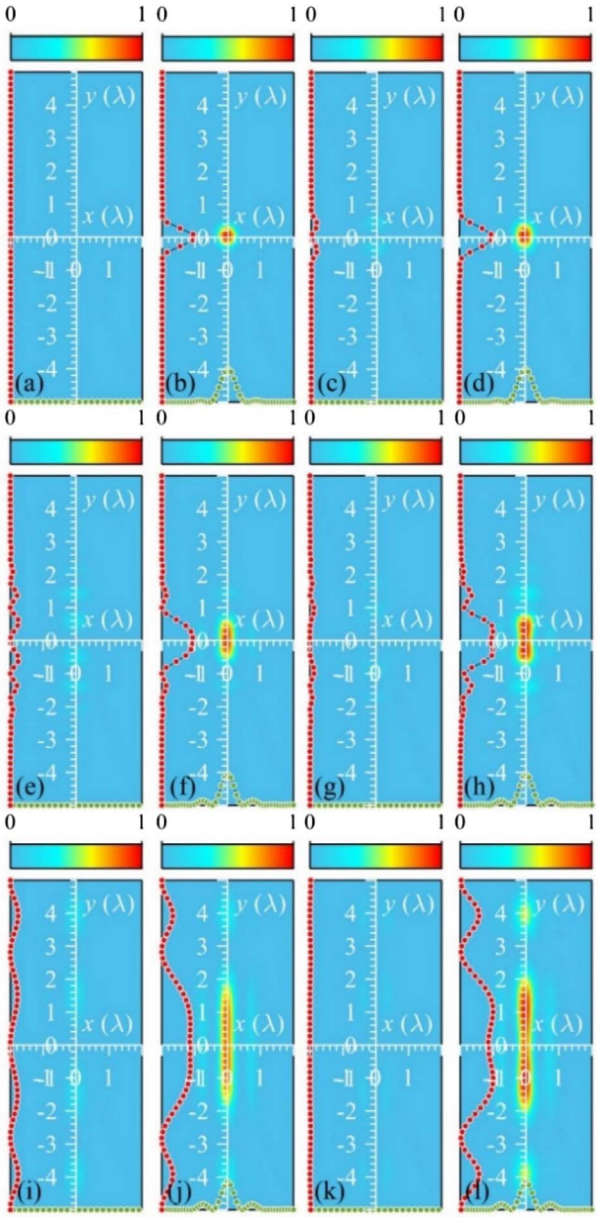

Fig. 2. Electric field intensity distributions of tightly focused input optical fields with $(v, c) = (0, \pi/2)$, $(1, \pi/2)$, and $(20, \pi/2)$ (upper, middle, and lower rows, respectively). From left to right, the four columns show the x-, y-, and z-polarized components and the total field. The insets for each image depict the normalized intensity profiles along the x (green curve) and y axes (red curve), respectively. All intensity distributions are normalized by the maximum intensity in the focal plane for each input light mode.

Such fascinating focal behaviors are attributed to the one-dimensional manipulation of the input SoPs. As a result, a transverse elongation of focus is also possible, complementing the well-known long depth of focus. Moreover, the long foci exhibit high uniformity as they are intensity profiles with near-flat tops; see insets in Figs. 2(h) and 2(l).

The value of the phase index v in the specially designed PB phase ε affects significantly the transverse enhancement of the focus, as seen in Fig. 2. To detail and quantify the relationship between v and the length and width of the focus, Fig. 3 shows

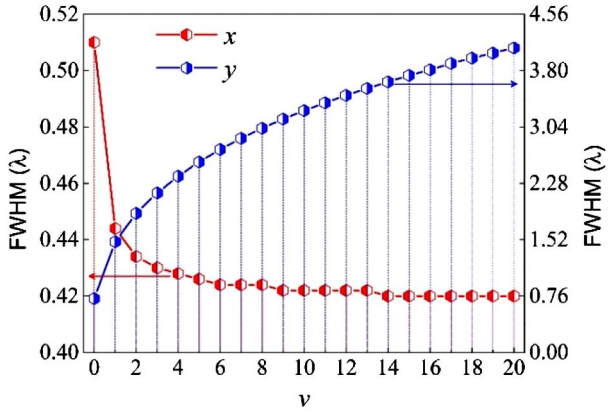

Fig. 3. Full width at half-maximum (FWHM) values along the x and y axes versus the phase index v with $NA = 0.95$.

the full width at half-maximum (FWHM) values along both the x and y axes versus v; the FWHW/λ values are from left to right ($v = 0, 1, \ldots, 20$): along the x axis, 0.510, 0.444, 0.434, 0.430, 0.428, 0.426, 0.424, 0.424, 0.424, 0.422, 0.422, 0.422, 0.422, 0.422, 0.420, 0.420, 0.420, 0.420, 0.420, 0.420, and 0.420, and along the y axis, 0.726, 1.492, 1.872, 2.150, 2.376, 2.568, 2.736, 2.886, 3.022, 3.146, 3.260, 3.366, 3.466, 3.560, 3.648, 3.734, 3.810, 3.896, 3.968, 4.036, and 4.106. Obviously, a linearly polarized beam may be used to create an elliptical spot under tight focusing conditions because this focal field has different FWHM values along these two orthogonal directions (the x and y axes). Furthermore, with increasing v, the FWHM values along the x axis (y axis) decrease (increase); they are smaller than the diffraction limit for this focusing lens $\lambda/(2\mathrm{NA}) = 0.526\lambda$ and different from the line-focusing of cylindrical lens. Therefore, a tunable transverse enhancement of focusing controlled by phase index v is achieved.

To provide a better understanding of the transverse enhancement of focusing assisted by the shaping of the PB phase, its energy flux needs to be evaluated. The corresponding three-dimensional magnetic field near focus may be similarly derived [20],

$$\mathbf{H}_{\mathrm{out}}(\rho,\phi,z) = \frac{-ikf\sqrt{\varepsilon/\mu}}{2\pi}\int_0^{2\pi}\int_0^{\alpha}\sqrt{\cos\theta}\,l_{\mathrm{in}}(\theta)\sin\theta\mathbf{M}_m \times e^{\{ik[-\rho\sin\theta\cos(\varphi-\phi)+z\cos\theta]\}}\mathrm{d}\varphi\mathrm{d}\theta, \tag{9}$$

$$\mathbf{M}_m = M_{mx}\hat{\mathbf{e}}_x + M_{my}\hat{\mathbf{e}}_y + M_{mz}\hat{\mathbf{e}}_z, \tag{10}$$

$$M_{mx} = -\cos\left[\varphi - 2\pi v\left(\frac{\sin\theta\sin\varphi}{\sin\alpha}\right)^3 - c\right]\sin\varphi + \sin\left[\varphi - 2\pi v\left(\frac{\sin\theta\sin\varphi}{\sin\alpha}\right)^3 - c\right]\cos\theta\cos\varphi, \tag{11}$$

$$M_{my} = \cos\left[\varphi - 2\pi v\left(\frac{\sin\theta\sin\varphi}{\sin\alpha}\right)^3 - c\right]\cos\varphi + \sin\left[\varphi - 2\pi v\left(\frac{\sin\theta\sin\varphi}{\sin\alpha}\right)^3 - c\right]\cos\theta\sin\varphi, \tag{12}$$

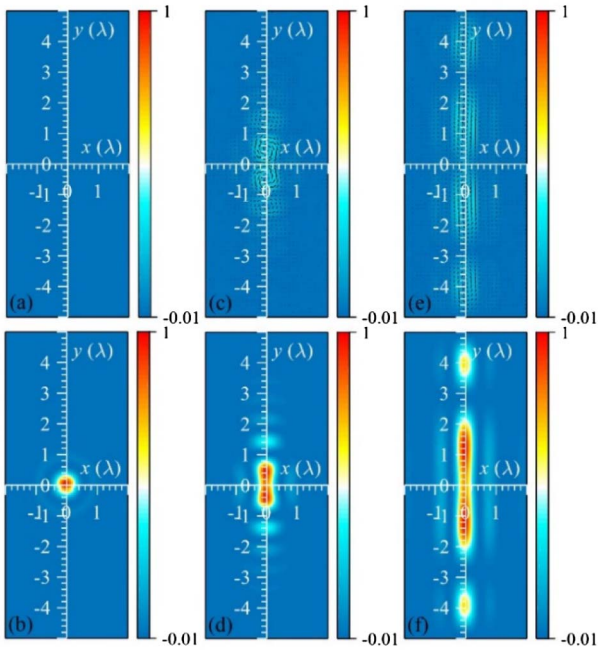

Fig. 4. Energy flow distributions of the tightly focused input optical fields with $(v, c) = (0, \pi/2)$, $(1, \pi/2)$, and $(20, \pi/2)$ (left, middle, and right columns, respectively). The upper and lower rows depict the transverse and longitudinal energy flows, respectively. The direction of the transverse energy flow is indicated by black arrows. All energy flow distributions are normalized by the maximum energy flow in the focal plane for each input light mode.

$$M_{mz} = \sin\left[\varphi - 2\pi v\left(\frac{\sin\theta\sin\varphi}{\sin\alpha}\right)^3 - c\right]\sin\theta, \tag{13}$$

where ε and μ denote, respectively, the dielectric constant and the magnetic permeability of the image space, and $\mathbf{M}_m$ is the magnetic field polarization vector in the image space. The magnetic fields' distributions described by Eqs. (9)–(13) are evidently quite different from those describing the electric fields, Eqs. (3)–(8). In terms of the three-dimensional electric and magnetic fields, the energy current is determined by the time-averaged Poynting vector [16,20],

$$\langle \mathbf{S} \rangle \propto \frac{c}{8\pi}\mathrm{Re}(\mathbf{E}_{\mathrm{out}} \times \mathbf{H}^*_{\mathrm{out}}). \tag{14}$$

Here, the asterisk represents the operation of complex conjugation. We can then calculate the energy flux based on Eq. (14).

The Poynting vectors of the transverse and longitudinal components in the focal plane for the fields (Fig. 2) are shown in Fig. 4. No transverse energy flow is found in Fig. 4(a). On the contrary, the circularly symmetric hot spot plays a dominate role in the longitudinal energy flow [see Fig. 4(b)]. However, with nonzero v, multiple rings in the transverse energy flowing along the y axis are very clearly observed exhibiting circular [Fig. 4(c)] and elliptical-shaped [Fig. 4(e)] patterns for low and high values of v, respectively. Moreover, the circular symmetry of the longitudinal energy flow is broken, becoming a needle-shaped pattern for v equal to 1 [Fig. 4(d)] and permitting a further elongation along the y axis with increasing v [Fig. 4(f)].

In conclusion, we have proposed a method to enhance the tightly focused field in the direction perpendicular to the optical axis assisted by a specially designed PB phase. The expression for calculating the electromagnetic and Poynting vector distributions near the focus has been derived using the Richards and Wolf vectorial diffraction methods. On the basis of an analytical model, the transverse enhancement was found to depend only on the phase index v in the PB phase. As a result, a focus with controllable length and subwavelength width in the focal plane has been achieved. Furthermore, the corresponding Poynting vector distributions were studied in detail. This work not only broadens the structured light fields, but also has potential applications that include optical microfabrication and nanofabrication, micromanipulation, and high-resolution layer-divided imaging.

Funding. National Natural Science Foundation of China (NSFC) (11604182); Natural Science Foundation of Shandong Province (ZR2016AB05).

REFERENCES

1. S. Pancharatnam, Proc. Indian Acad. Sci. A **44**, 247 (1956).
2. M. V. Berry, J. Mod. Opt. **34**, 1401 (1987).
3. R. Bhandari, Phys. Rep. **281**, 1 (1997).
4. T. van Dijk, H. F. Schouten, W. Ubachs, and T. D. Visser, Opt. Express **18**, 10796 (2010).
5. J. Samuel and R. Bhandari, Phys. Rev. Lett. **60**, 2339 (1988).
6. T. F. Jordan, Phys. Rev. A **38**, 1590 (1988).
7. M. V. Berry, Phys. Today **43**(12), 34 (1990).
8. Z. Bomzon, V. Kleiner, and E. Hasman, Opt. Lett. **26**, 1424 (2001).
9. J. P. Balthasar Mueller, N. A. Rubin, R. C. Devlin, B. Groever, and F. Capasso, Phys. Rev. Lett. **118**, 113901 (2017).
10. H. Wang, L. Shi, B. Lukyanchuk, C. Sheppard, and C. T. Chong, Nat. Photonics **2**, 501 (2008).
11. F. Maucher, S. Skupin, S. A. Gardiner, and I. G. Hughes, Phys. Rev. Lett. **120**, 163903 (2018).
12. T. Bauer, P. Banzer, E. Karimi, S. Orlov, A. Rubano, L. Marrucci, E. Santamato, R. W. Boyd, and G. Leuchs, Science **347**, 964 (2015).
13. F. Bouchard, H. Larocque, A. M. Yao, C. Travis, I. D. Leon, A. Rubano, E. Karimi, G. Oppo, and R. W. Boyd, Phys. Rev. Lett. **117**, 233903 (2016).
14. P. Li, X. Guo, S. Qi, L. Han, Y. Zhang, S. Liu, and J. Zhao, Sci. Rep. **8**, 9831 (2018).
15. Z. Man, C. Min, L. Du, Y. Zhang, S. Zhu, and X. Yuan, Opt. Express **24**, 874 (2016).
16. V. V. Kotlyar, A. A. Kovalev, and A. G. Nalimov, Opt. Lett. **43**, 2921 (2018).
17. S. Liu, P. Li, and J. Zhao, Proc. SPIE **10549**, 105491A (2018).
18. Q. Zhan, Adv. Opt. Photon. **1**, 1 (2009).
19. X.-L. Wang, J. Chen, Y. Li, J. Ding, C.-S. Guo, and H.-T. Wang, Phys. Rev. Lett. **105**, 253602 (2010).
20. B. Richards and E. Wolf, Proc. R. Soc. A **253**, 358 (1959).
21. K. Youngworth and T. Brown, Opt. Express **7**, 77 (2000).